Computers and Electronics in Agriculture 174 (2020) 105496

Contents lists available at ScienceDirect

Computers and Electronics in Agriculture

journal homepage: www.elsevier.com/locate/compag

In-field machine vision system for identifying corn kernel losses

Nolan S. Monhollen, Kevin J. Shinners*, Joshua C. Friede, Eduardo M.C. Rocha, Brian L. Luck

University of Wisconsin, Department of Biological Systems Engineering, United States

ARTICLE INFO

Keywords:
Corn losses
Imaging
Machine vision

ABSTRACT

Losses from the combine corn header result in decreased yield and profit. The development of improved corn headers to reduce losses is hampered by lack of sufficient tools for kernel loss assessment. A loss assessment system was developed that consisted of a residue clearing process to expose lost corn kernels on the ground, and a machine vision image system to quantify the exposed kernels. A mower deck was used to size-reduce and remove residue with minimal kernel displacement. The vision system consisted of an optical system for imaging the ground area and an image analysis program to identify lost kernels.

The image analysis corn kernel detection system achieved an average precision of 0.90. A further assessment of system accuracy using random images from additional field tests resulted in an accuracy of 0.91. The combined residue clearing and machine vision systems achieved an overall system accuracy of 0.82 in field tests evaluating staged losses using known quantities of kernels. The loss analysis system was able to distinguish statistically significant ($P < 0.05$) differences in losses created by different corn header deck plate spacing, while requiring less time and labor than conventional assessment methods.

1. Introduction

Corn kernel losses from the combine harvester result in decreased yield and profit, create problems with volunteer corn, and serve as overwintering sites for pathogens with potential to harm subsequent crops (Hanna, 2010). Losses from the combine harvester corn header often account for the largest portion of total machine losses (Hanna et al., 2002; Paulsen et al., 2014). Machine factors that can affect kernel loss at the header would include, but not be limited to, deck plate spacing, header operating speed, header alignment with the ground contour, and harvester speed (Shauck and Smeda, 2011; Pishgar-Komleh et al., 2013; Monhollen, 2020). Measuring kernel loss at the header usually involves counting kernels on the ground in a given area or laying tarps in the rows prior to harvest to collect lost kernels (Hanna et al., 2002; Monhollen, 2020). Both methods are labor intensive and time consuming so they are difficult to use in experiments with many variables and replicates. Additionally these systems have limited area of collection, typically less than 3 m^2 per replicate. A system that provided precise, fast estimates of lost corn kernels over a large collection area would provide better assessments of corn header performance. Ultimately such a system could be used to detect losses during harvest and real-time machine adjustments made to reduce these losses.

Previous research has shown that vision systems can be used to analyze corn kernels to estimate quality, detect kernel defects and damage, and estimate physical properties (Valiente-Gonzalez et al., 2014; Orlandi et al., 2018; Li et al., 2019). For instance, a camera and hardware based image analysis system was able to inspect of up to 75 kernels s^{-1} at an accuracy of 91% (Pearson, 2009). Most of these systems required the corn kernels to be placed in laboratory fixtures where kernels were hand separated so they do not touch since touching kernels were not segmented accurately (Li et al., 2019).

More recently systems have been developed that do not require separation of kernels. A vision system was developed to identify kernels fragments to assess level of kernel size-reduction in whole-plant corn silage without requiring separation of kernels from the non-grain fractions (i.e. stalk, husk, cob and leaves) (Rasmussen and Moeslund, 2019). Other systems have been developed that detect broken grain from a mass of grain flowing in the clean grain elevator of combine harvesters (Escher and Krause, 2014; Pezzementi et al., 2016). However, there has not been previously published research on using vision systems to detect corn kernels lost to the ground during harvest. A major challenge of this task is that plant residue must first be cleared to expose, but not displace, the kernels on the ground. Therefore, the objectives of this research were to develop a complete system to determine corn kernel losses caused by the combine harvester corn header. This system would include a residue clearing system to reveal lost kernels on the ground and a machine vision image system to quantify the kernels lost. A final objective would be to use the

* Corresponding author at: 460 Henry Mall, Madison, WI 53706, United States.
E-mail address: kjshinne@wisc.edu (K.J. Shinners).

https://doi.org/10.1016/j.compag.2020.105496
Received 31 January 2020; Received in revised form 4 May 2020; Accepted 7 May 2020

developed system to quantify corn kernel losses as affected by corn header deck plate spacing.

2. Residue clearing system

Quantifying corn kernels on the soil surface required removing residue without disrupting or moving the corn kernels below. Several residue clearing methods were investigated including air entrainment, mechanical transport, and a combination of the two (Monhollen, 2020). Ultimately the residue was removed using a combination of size-reduction and vacuum by using a John Deere (Moline, IL) model HC54 mower deck and associated X758 tractor. The mower blades cut the remaining crop stubble, size-reduced the residue, lifted the detached residue by the vacuum created by the rotating blades, and then ejected the residue laterally from the row of interest. The mower was equipped with a 137 cm wide deck and was configured with three conventional mower blades (part number M164016) operated at 3517 rev·min^{-1}. A cutting blade height of approximately 6 cm was used. Kernels that do not fall to the ground but are located within the residue would be displaced by this system, resulting in an under estimate to true kernel losses.

3. Machine vision hardware

The system hardware consisted of a transport trailer, a machine vision camera and lens, a rotary encoder and microcontroller to measure image spacing, a host computer for image acquisition control and data processing, a supportive frame and covers for protection of the camera and control of ambient lighting, and an auxiliary lighting system (Fig. 1).

The trailer was designed so that no frame members would interfere with the defined image region of interest (ROI) which consisted of an area 101 cm long and 76 cm wide which extended 38 cm to each side of the evaluated corn row. Camera height and trailer pitch were adjustable to ensure a level imaging plane. A wheel-driven rotary encoder (Koyo Electronics Industries Co. model TRD-N500-RZWD, Kodiara, Japan) was utilized to measure distance traveled between images.

A lighting system was used to provide the consistent light intensity required for the 400 μs exposure time used. Ten LED light pods (model WL-15W, Super Bright LEDs Inc., St. Louis, MO) of 780 lm intensity and 6000 K color temperature were fixed in a bright-field format. The lights used a 45 degree beam angle lens and were oriented to minimize variation in light intensity across the imaged area. The lights were positioned in parallel with the camera lens plane.

The machine vision camera was a FLIR model Blackfly S GigE (FLIR Systems, Wilsonville, OR) 12MP RGB with a 1/1.7 in. CMOS photodetector and rolling shutter capable of 2.5 fps at the maximum specified image resolution (4000 × 3000 pixels) with an exposure range of 10 μs

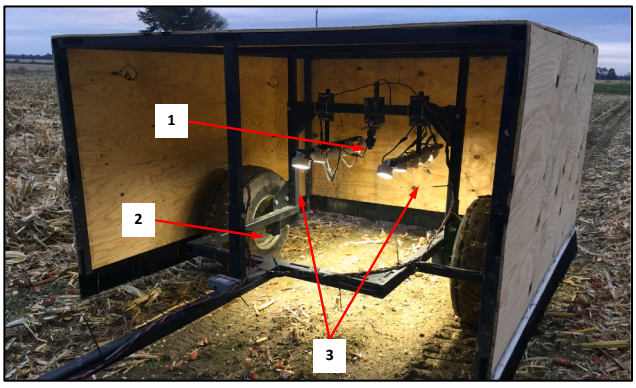

Fig. 1. Imaging system showing: (1) machine vision camera, (2) wheel-driven rotary encoder, and (3) auxiliary light system. Front cover removed.

to 30 s. Image data transfer used a combination of FLIR Spinnaker SDK software and MATLAB (Mathworks, Natick, MA) Image Acquisition Toolbox. The manually adjustable lens was a Theia Technologies (Theia Technologies, Wilsonville, OR) model SL410 which provided focus, zoom, and iris control.

The imaged area was originally calibrated by adjusting camera zoom and focus to view an area that was 76 cm wide (i.e. corn row spacing) at the centermost point of the image. However, this resulted in an actual imaged area that was larger than the desired image area of 0.767 m^2 (1.01 × 0.76 m) due to image distortion. An image of a checkerboard with known grid dimensions was acquired and image processing performed to correct image distortion before calculating actual imaged area. Actual image area as a result of image distortion was determined to be 0.983 m^2.

Image acquisition was triggered in response to a signal provided by the position of the camera cart wheel at defined intervals. Wheel rotation was measured by the rotary encoder, and its output converted into relative position using an Arduino (Adafruit Industries, New York, NY) Nano microcontroller. Connection with the host computer was utilized through USB serial communication by use of the MATLAB Support Package for Arduino.

4. Faster R-CNN and image training

Detection and classification of corn kernels within the acquired training images was performed using a corn kernel detection program developed using a Faster Regions with Convolutional Neural Networks (Faster R-CNN) for purposes of object detection (Fig. 2). An existing CNN that was pre-trained using the ImageNet database (Deng et al., 2009) was retrained for corn kernel detection to minimize the number of training examples required to approach the desired accuracy of 95%. In this study, the publicly available Resnet-50 CNN architecture was selected to utilize the significant number of network layers afforded by residual network connections (He et al., 2016). Retraining and implementation of the existing Resnet-50 CNN was performed using the MATLAB Deep Learning Toolbox Model for ResNet-50 Network.

To detect corn kernels, a Faster R-CNN detector was chosen to utilize a region proposal network (RPN) which shares convolutional layers with the object detection network, utilizing anchor boxes to propose features before classifying these features by predefined class (Ren et al., 2015) (Fig. 2). The RPN proposed regions by evaluating the feature maps from earlier feature extraction layers in the Faster R-CNN. Initial assessment of the likeliness of an area to be a region of interest (i.e. corn kernels) was performed by the RPN by assessing the image in parts using a sliding window technique. Bounding boxes were proposed for areas of the image above a certain threshold of likeliness to contain a corn kernel. The bounding box regions were pooled and sent to the remaining layers of the Faster R-CNN where they were classified depending on whether or not a corn kernel represented an object class being assessed. The RPN did not classify objects, but rather suggested regions of possible feature locations to minimize the unnecessary classification of areas of the image that were unlikely to contain an object, resulting in a faster detection process.

Implementation of a Faster R-CNN detector determined data for the detected object class and confidence, as well as a bounding box representing object location and an estimation of object size in the image. The Faster R-CNN was trained as five epochs with an initial learn rate of 1.0 × 10^{-3} and a mini-batch size of one.

Retraining of the network for the detection of corn kernels utilized datasets of actual images created for the specific application of detecting corn kernels on the soil. This ground truth data was selected to provide examples of common in-field loss scenarios expected to be encountered during harvest, as well as unusual field conditions that sought to increase the diversity of this machine vision application.

Ground truth image collection was conducted using different conditions of soil moisture, soil type, residue quantity, light intensity,

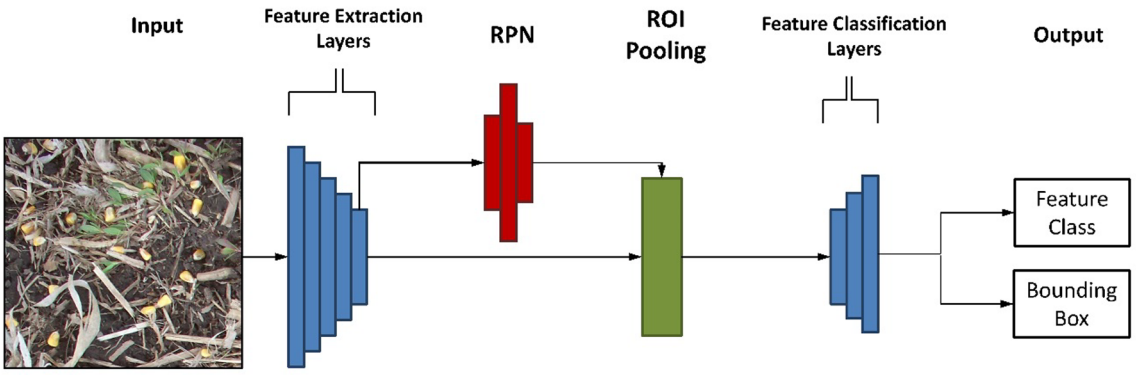

Fig. 2. Schematic of Faster R-CNN utilizing a region proposal network (RPN) used to determine regions of interest (ROI) for detection and classification of corn kernels within images.

ground cover type and quantity, and kernel moisture, quality, and size. Images collected for training and validation of the Faster R-CNN represented a random distribution of kernels representative of typical header losses. Ground truth RGB images were captured using handheld and cell phone cameras and the machine vision camera (all 12MP − 3000 × 4000 pixel resolution). In a similar fashion to Montalvo et al. (2016), each 12 MP ground truth image collected for the purposes of training was divided into 12 equal subset images of 1000 × 1000 pixels to simplify annotation of the ground truth image data.

Creation of ground truth data was performed manually using the MATLAB Image Labeler. A single label was used to define kernels as objects for all ground truth image subsets. Object selection consisted of a box placed around the outer boundaries of the kernel. Ground truth data was not stored as image pixels, but rather stored as metadata of kernel location corresponding to area coordinates within the specified subset image (Fig. 3). This coordinate metadata was then referenced during training.

A total of 299 ground truth images were subdivided into 3588 subset images containing approximately 25,000 manually annotated kernel instances. These subset images were utilized in training and validation of the image analysis program, with 80% (2,870) of the images used for training and 20% (718) used for validation. The subset images were randomly assigned to either the training or validation datasets with each image being assigned to only one dataset to ensure uniqueness.

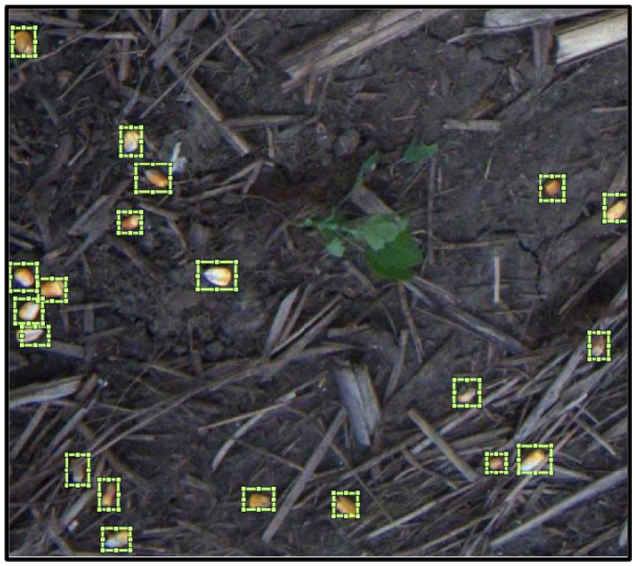

Fig. 3. Example of ground truth data subset containing labeled region of interest (ROI) objects of a single class representing individual kernels.

Validation of the accuracy of the image analysis program was performed by assessment of the Average Precision (AP) metric. Validation images were processed by the program and a comparison was made between generated and manually drawn boundary boxes. A False Positive (type 1 error) was defined as a kernel identified by the program that did not have a manually derived box associated with it. A False Negative (type 2 error) was defined as a manually identified kernel that was not detected. A True Positive occurred where the program and manual boundary boxes agreed. Precision was defined as the ratio of the True Positives to the sum of all positive instances of objects determined by the program (eqn. 1). Recall was defined as the ratio of True Positives to the sum of the True Positives and False Negatives (eqn. 2). Average Precision was defined as the average of the evaluated precision for recall values from 0 to 1 (eqn. 3).

An additional assessment of image analysis accuracy was done using a group of subset images randomly selected from the deck plate spacing experiments (see section 5.2). Each subset image was processed and evaluated for type 1 and type 2 errors. Two separate, independent manual assessments were then performed on the same group of subset images by individuals trained to identify kernels and assess image analysis accuracy. This was done by assessing the program identified bounding box locations to determine if they represented kernels and quantifying any mistakes made (type 1 errors), and then quantifying any kernels in the image that were not identified by the program (type 2 errors). A metric defined as the Combined Accuracy (CA) was calculated to quantify the combined impact of type 1 and 2 errors. The CA was an assessment of error in comparison to a typical trained human ability to detect kernels. The CA was determined for each subset image by subtracting the False Positives (type 1 errors) from the True Positives and finding the proportion relative the sum of the True Positives and the False Negatives (type 2 errors) (eqn. 4). An average CA for all subset images was determined for both assessors.

$$P = T_P/(T_P + F_P) \quad (1)$$

$$R = T_P/(T_P + F_N) \quad (2)$$

$$AP = \int_0^1 P(R)dR \quad (3)$$

$$CA = (T_P - F_P)/(T_P + F_N) \quad (4)$$

where:

P Precision of the image analysis kernel detector
R Recall of the image analysis kernel detector
AP Average precision of the image analysis kernel detector
T_P True positive
F_P False positive (type 1 error)
F_N False negative (type 2 error)
CA Combined accuracy of the image analysis kernel detector

5. Materials and methods

5.1. Staged loss experiments

The staged loss experiments were conducted to determine the effectiveness of the combined residue clearing and the kernel detection machine vision systems. Experiment No. 1 was conducted in WI (43.3380°, 89.3804°) and Experiment No. 2 conducted in IN (39.5859°, 85.8636°). The fields were first harvested so that only three adjacent rows were left standing. The ears of these rows were then removed by hand for a distance of approximately 60 m. These two methods were used to insure there were no lost kernels in the image area prior to imaging. Kernels were then placed by hand within the camera system image area (0.983 m^2) and distributed approximately evenly on either side of the center row. Quantities of dispersed kernels per replicate (16 and 32 replicates in Experiments No. 1 and 2, respectively) were randomly varied between 20 and 100 kernels at a consistent spacing of 1.8 m between image centers. A combine harvester with a non-chopping corn header was then used to harvest the three rows in such a way that there was no wheel traffic in these rows. The hand dispersed kernels were consequently covered with residue as would be typical during normal harvesting.

The residue clearing mower was then used to clear residue across all replicates locations collectively. The outside two rows were cleared first by traveling axial to the row with the material directed away from the center row, before the center row was then cleared. This progression was used so that residue cleared from the row of interest would not be impeded by stalks and residue in the adjacent rows. A consistent ground speed of approximately 2 km h^{-1} was used for all operations and the mower blade cutting height was set to approximately 6 cm.

Two (Experiment No. 2) or three (Experiment No. 1) residue clearing operations were performed, with images captured after each clearing operation. Images were captured at each of the replicate locations with the camera system stationary and the camera centered above the defined image area. Processing of each image was performed using the image analysis program, and the estimated quantity of kernels in each image determined at 0.90 and 0.95 confidence.

A System Accuracy (SA) was calculated to quantify the combined accuracy of the residue clearing and machine vision systems. Under identifying the known number of kernels could be attributed to residue still covering kernels, the residue clearing mower displacing kernels, or the image system not detecting uncovered kernels (type 2 error). Over identifying the known number of kernels would be a type 1 error of the image system. The method of calculating SA (eqn. 5) assessed both under and over quantification of kernels relative to the known number of hand placed kernels as an absolute error and therefore accounted for both equally.

$$SA = 1 - (|K_{KN} - K_D|/K_{KN}) \quad (5)$$

where:

SA System accuracy at each image location.
K_{KN} Known quantity of kernels placed at each image location.
K_D Quantity of kernels detected by the image system.

Mean SA was calculated for staged images after each residue clearing operation. Standard error of the mean (SEM) was calculated for each mean SA. A one-way analysis of variance was performed using Excel to determine difference between sample means within each experiment.

5.2. Deck plate spacing experiments

An important use of the developed system is to assess corn header performance with regard to kernel loss. Previous research has shown that deck plate spacing was very influential in header losses (Quick, 2003; Monhollen, 2020). Therefore, evaluation of losses as a result of different deck plate spacings was assessed by the residue clearing plus the machine vision systems. Experiment No. 3 was conducted in IN (39.5859°, 85.8636°) and Experiment No. 4 conducted WI (43.3380°, 89.3804°). Experiment No. 3 used a 12-row Claas (Harsewinkel, Germany) model 12–30 non-chopping corn header and Experiment No. 4 used a 12-row John Deere model 612C chopping corn header. Deck plate spacings of 29, 37, and 44 mm were used for both experiments and spacing was measured at the beginning of the fluted section of the stalk rolls.

Each experiment consisted of nine plots each 50 m long. In Experiment No. 3 all nine plots were aligned end to end and arranged in three blocks. Each block had three plots in which the three deck plate spacings were randomly assigned. Experiment No. 4 was similar except that the three blocks were arranged side-by-side rather than aligned end to end. The combine harvester was configured with the chopper of the residue distribution system disabled so that kernels lost from the back of the combine would not be thrown into the data rows (see below). The combine harvester was operated at approximately 6.4 km·h^{-1}.

Of the 12 harvested rows, rows 2 and 11 were selected for assessment. The residue clearing procedure described in section 5.1 was performed for all test plots after all the plots had been harvested. After imaging, the residue clearing procedure was again applied on rows 2 and 11 and another set of images collected.

Each of the two rows imaged was considered a replicate row with 20 images collected per row, so 40 images were collected per plot. Since there were three replicate plots for each deck place spacing, there were 120 images per deck plate spacing and a total of 360 images collected. After all 360 images were collected, the residue clearing mower was operated over the data rows again and the image taking process was repeated resulting in an additional 360 images. Care was taken to prevent any wheel traffic in the data collection rows from the combine or the residue clearing mower.

Image collection was performed while moving at a ground speed of 2.4 km·h^{-1}. Images were captured at a spacing of 1.5 m controlled by the imaging control system. Camera settings were not altered and all images were taken using a camera exposure of 400 μs. Evaluation of the images was performed post-collection to allow for rapid image collection during experiments. Post-processing of images was automated and outputs calculated as a quantity of kernels present within each image at 0.90 and 0.95 confidence. Specific mass of estimated kernel loss was determined using image area (0.983 m^2) and converting kernel quantity to a mass basis by using a conversion of 90,000 kernels per 25.4 kg (Nielsen, 2018).

Average kernel specific mass (i.e. kg ha^{-1}) for each replicate was determined from the 40 images taken per plot and the SEM calculated. Comparison between sample means of the three deck plate spacings for all replicates was performed using Tukey's Honest Significant Difference (HSD) using JMP Pro (ver. 13.1, SAS Institute Inc., Cary, N.C.). Using calculated sample means and variances for the three deck plate spacings, an assessment of the number of images required to determine statistical significance between the three deck plate spacings was made. To determine sample size, an independent two sample *t*-test was performed between the three comparable spacings for a target significance level of 0.05. The required sample size (i.e. degrees of freedom) was determined by the t statistic required to exceed this significance level.

6. Results

6.1. Machine vision accuracy

The AP (eqn. 3) of the image analysis system was 0.90 using the validation dataset. An ideal detector achieves a precision and recall of 1 (AP = 1), resulting in a square precision-recall plot. The precision-recall plot for the validation dataset approximated this ideal shape,

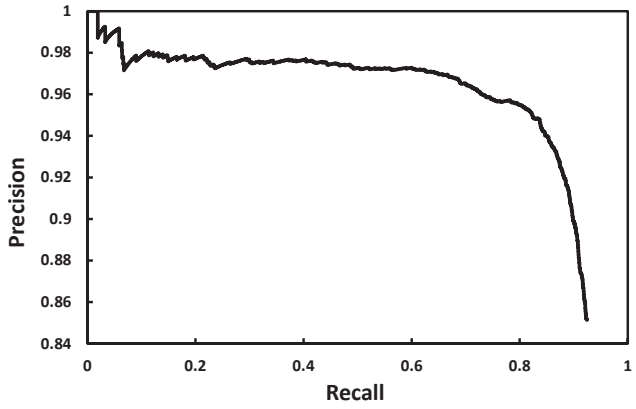

Fig. 4. Precision-Recall curve for final iteration of image analysis system for the validation dataset of 718 images.

achieving good precision even at greater recall values, meaning it detected kernels with high confidence without a significant number of missed kernels (Fig. 4). Assessment of CA (eqn. 4) consisting of random images collected during deck plate spacing experiments was 0.91. This assessment reinforces the accuracy of the image analysis system on images beyond those assessed in the validation dataset.

6.2. Staged loss experiments

Average SA (eqn. 5) for the staged loss experiments was between 0.58 and 0.86 (table 1). Analysis using greater confidence generally resulted in lower accuracy because the analysis was more conservative. In one case the system accuracy was greater at greater confidence likely because there were fewer false positives.

Average SA after one residue clearing operation was 0.58 and 0.80 for the Experiment No. 1 and No. 2, respectively (table 1). It was observed that long stalks were left after the first clearing operation with Experiment No. 1 which made identifying kernels more difficult (Fig. 5). Residue was more thoroughly removed with a single clearing operation in Experiment No. 2 which accounts for the better SA in this experiment (Fig. 5).

The SA considerably improved after the second residue clearing operation in Experiment No. 1 but accuracy numerically declined in Experiment No. 2 (table 1). The second residue clearing operation in Experiment No. 1 removed many long stalks left after the first operation, so more kernels were uncovered and the SA improved. The reduction in SA after the second clearing operation with Experiment No. 2 could have been the result of kernels being displaced out of the image area by the mower blades. To quantify the extent of kernel displacement, future tests would require that kernels be hand counted in the image area after residue clearing and image analysis.

Table 1
Average System Accuracy (eqn. 5) of the complete kernel loss analysis system using staged kernel images for varying number of residue clearing operations.

Number of Residue Clearing	Average System Accuracy			
Operations	0.90 CI [a]	SEM	0.95 CI [a]	SEM
Experiment No. 1[b]				
One	0.58b	0.05	0.52c	0.05
Two	0.80a	0.03	0.76b	0.03
Three	0.82a	0.03	0.86a	0.03
LSD (P = 0.05)[c]	0.10		0.09	
Experiment No. 2[b]				
One	0.80a	0.02	0.76a	0.02
Two	0.78a	0.02	0.75a	0.02
LSD (P = 0.05)[c]	0.05		0.05	

[a] CI is the Confidence Interval defined by the image analysis program.
[b] Number of replicate images was 16 and 32 for Experiments No. 1 and 2, respectively.
[c] Least square difference. Averages in columns with different letters are significantly different at 5% significance level.

In Experiment No. 1 the residue cover left after the third clearing operation was only slightly improved from that after the second clearing operation, so the SA did not significantly increase (0.90 CI). It was observed that in Experiment No. 1, the residue cover left after two or three clearing operations was similar to that left after a single operation in Experiment No. 2. The soil and residue conditions were not quantified, but were considered to be typical “wet” and “dry” harvest conditions in Experiments No. 1 and 2, respectively. This likely accounted for differences in effectiveness of the residue clearing system between experiments.

Because the residue clearing performance can be variable with crop and environmental conditions, in the future it might be useful to develop an associated residue detection system and specify that kernel losses be quantified only when the residue cover is below a minimum threshold. Alternatively, assessment of residue cover could be part of the machine vision system, determining the quantity of kernels visible in relation to the portion of the imaged area covered by residue thereby accounting for the visibility of kernels in the image when assessing losses.

6.3. Deck plate spacing experiments

The SEM for losses at 29 and 37 mm deck plate spacings showed small variability between replicates while the losses at the 44 mm setting were much more variable (Fig. 6). This result was similar for both Experiments No. 3 and 4 (data not shown). Accuracies assessed for the image analysis system using known kernel quantities (see section 6.2) suggest that the variability of loss at 44 mm spacing was likely the result of spatial variability rather than solely image system variability (Fig. 7). Estimated kernel loss was significantly affected by deck plate spacing with dramatic increases when spacing was increased from 37 to 44 mm (Figs. 8 and 9). Corn ears are tapered with the smallest diameter at the tip and generally the largest diameter near the middle of the ear. Once the deck plate spacing exceeds some portion of the ear diameter, shelling of kernels by the counter-rotating stalk rolls can occur. Shelling in this manner will depend on orientation of the ear as it approaches the deck plate (i.e. base or tip first) and the diameter of the ear relative to deck plate spacing. Storck et al. (2007) sampled 280 corn ears across seven different hybrids and reported that average maximum ear diameter varied from 45.8 mm ± 2.4 mm to 51.2 mm ± 2.7 mm. Monhollen (2020) reported base and middle diameters of 120 ears of 43 mm ± 3.5 mm and 47 mm ± 3.3 mm, respectively. These results show why kernel loss can be very dependent on even small changes in deck plate spacing and can vary as ear size changes spatially due to agronomic conditions.

Estimated loss of kernels increased when images were taken after the second residue clearing operation in Experiment No.1 (Fig. 8) where estimated losses were greater by 44%, 30% and 19% for 29, 37 and 44 mm deck plate spacing, respectively. The second residue clearing operation evidently uncovered additional kernels that were hidden by residue after a single clearing operation, providing a better estimate of losses. This was not the case for Experiment No. 4 where a single residue clearing operation would have been sufficient to estimate corn head losses (Fig. 9).

Losses were greater with the chopping corn head (Experiment No. 3) than the non-chopping corn head (Experiment No. 4), but a direct comparison is not appropriate because the experiments were not conducted at the same time or with the same crop conditions. In Experiment No. 3 the estimated losses at 90% confidence varied from 236 to 630 kg ha^{-1} (3.7 to 10.0 bu ac^{-1}) at 44 mm deck plate spacing while losses at 29 and 37 mm spacing did not exceed 112 kg ha^{-1} (1.8 bu ac^{-1}). Average yield was 14,350 kg ha^{-1} (227.5 bu ac^{-1}) so losses

Fig. 5. Comparison of residue remaining after one (left) or three (middle) residue clearing operations in Experiment No. 1 and a single clearing operation in Experiment No. 2 (right). Configuration of residue clearing mower was the same for both experiments. Dashed yellow lines represent the approximate center of the rows where images were taken.

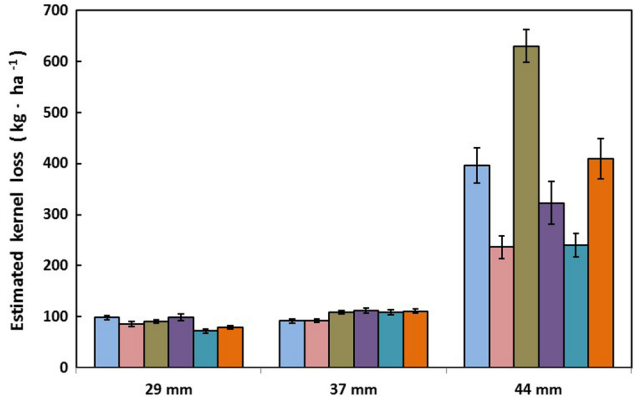

Fig. 6. Estimated kernel loss with a non-chopping corn head (Experiment No. 3) using 29, 37 and 44 mm deck plate spacing after two residue clearing operations and then use of the machine vision image analysis system at 90% confidence. Each bar represents one replicate plot in which 20 images were used to estimate losses. Error bars represent SEM.

ranged from 0.8% to 4.4% of yield. In Experiment No. 4 the estimated losses at 90% confidence varied from 540 to 1156 kg ha^{-1} (8.6 to 18.4 bu ac^{-1}) at 44 mm deck plate spacing while losses at 29 and 37 mm spacing did not exceed 176 kg ha^{-1} (2.8 bu ac^{-1}). Average yield was 10,920 kg ha^{-1} (173.0 bu ac^{-1}) so losses ranged from 1.6% to 10.6% of yield. Average losses using the manual tarp method were 35 and 400 kg ha^{-1} (0.6 to 6.4 bu ac^{-1}) for deck plate spacing of 35 and 43 mm, respectively (Monhollen, 2020). Losses determined by collecting lost kernels from the soil were 50 to 110 kg ha^{-1} (0.8 to 1.7 bu ac^{-1}) for an unspecified deck plate spacing (Hanna et al., 2002).

An evaluation of required sample size to achieve statistical significant differences between losses at different deck plate spacings of 29 vs.44 mm and 37 vs. 44 mm spacing could be found in as few as 3 to 6 images (Table 2). Determining the differences between 29 vs. 37 mm spacing however required between 10 and 38 images. The sensitivity of the system was such that significant differences in kernel loss between 29 and 37 mm deck plate spacing were determined in both experiments (Figs. 8 and 9). This was not the case in a similar experiment using the same corn head and the tarp collection method where six replicate sampling locations were used (Monhollen, 2020).

Measuring kernel loss frequently involves hand sampling lost kernels from an area that is less than 3 m^2 (Hanna et al., 2002; Monhollen, 2020) and sometimes as small an area as 0.25 m^2 (Pishgar-Komleh

Fig. 7. Spatial variability in kernel loss after harvest with corn header using 44 mm deck plate spacing after one residue clearing operation (Experiment No. 4). Note that kernel loss is moderate (blue outline); then heavy (green outline); then light (red outline).

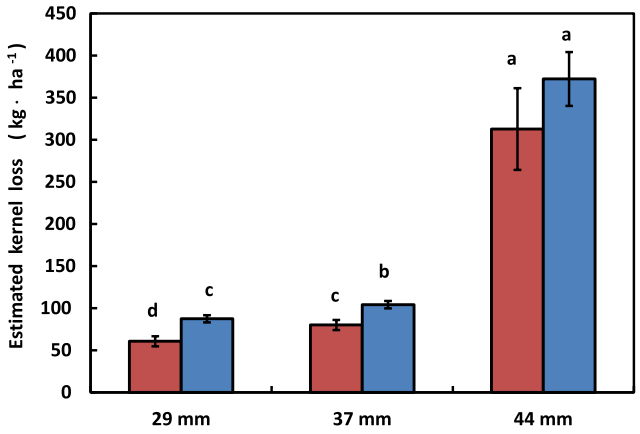

Fig. 8. Estimated kernel loss with a non-chopping corn head (Experiment No. 3) using 29, 37 and 44 mm deck plate spacing after one (red bars) or two (blue bars) residue clearing operations and then use of the machine vision image analysis system at 90% confidence. Each bar represents the average of 120 images, error bars represent SEM and averages with different letters are statistically different at 5% significance level.

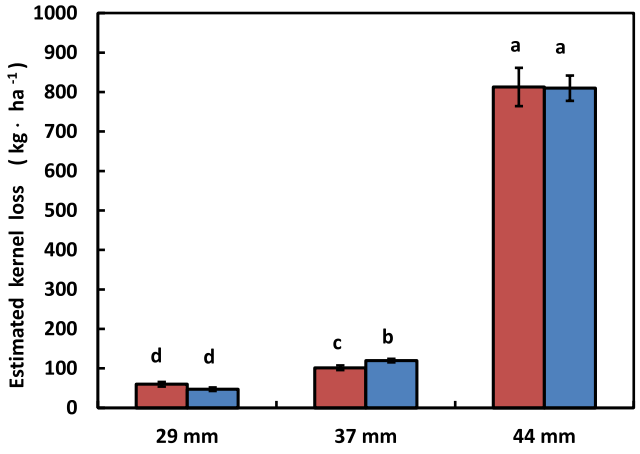

Fig. 9. Estimated kernel loss with a chopping corn head (Experiment No. 4) using 29, 37 and 44 mm deck plate spacing after one (red bars) or two residue clearing operations and then use of the machine vision image analysis system at 90% confidence. Each bar represents the average of 120 images, error bars represent SEM and averages with different letters are statistically different at 5% significance level.

Table 2
Required number of images to establish a significant difference at significance level of 5% using image analysis program at 0.95 confidence.

Comparison of Deck Plate Spacings	Number of Residue Removal	Number of Images Required	
(mm)	Operations	Exp. 3[a]	Exp. 4[a]
29 vs. 44	One	6	3
37 vs. 44	One	6	3
29 vs. 37	One	17	19
29 vs. 44	Two	6	4
37 vs. 44	Two	5	4
29 vs. 37	Two	38	10

[a] Experiments No. 3 and 4 were performed with a non-chopping and chopping corn headers, respectively.

et al., 2013). These systems are labor intensive, tedious and take so long that limited replicates can be conducted during a time when crop conditions are similar. For instance Hanna et al. (2002) and Pishgar-Komleh et al. (2013) reported losses using only four replicate samples per experimental treatment. The imaging system developed here takes images that were each approximately 1 m^2. The loss estimated for each deck plate spacing represented in Experiments No. 3 and 4 represent loss assessments over approximately 120 m^2, or more than 10 times the total assessment area of the manual systems referenced above. For each number of residue clearing operations used, the data was collected in one day by a single-person. The spatial variability of the loss data at 44 mm deck plate spacing shows the value of the large total sampling area possible with the developed system. When labor intensive systems limit the number measurements to only a few replicates, it is possible that data bias can occur.

Assessment of losses for purposes of corn header development appears to be feasible with the current status of the residue clearing and corn kernel loss analysis systems. Implementation for this purpose would require assessment of crop conditions to determine the required configuration of the residue clearing mower (i.e. mower deck height, mower ground speed, and number of clearing operations). This assessment could be done qualitatively or could be based on quantified criteria. For instance, a test similar to the staged kernel tests could be conducted and the mower configuration could be chosen that achieves a determined accuracy. Tests on different header configurations could then proceed and subsequent loss measurements would use this consistent residue clearing mower configuration. Alternatively, detection of residue cover could be part of the system so that kernel detection would only proceed when the residue cover in the imaged area is less than a predetermined value. An additional feature to detect lost whole or partial corn ears would also add value to the developed system.

7. Conclusions

The Faster R-CNN machine vision image analysis system achieved an average precision (AP) of 0.90. This value was assessed over a range of validation images in conditions beyond those typically found during harvest and supports the robustness of this application for corn kernel detection. A further assessment of system accuracy using random images from the deck plate spacing experiments resulted in an accuracy of 0.91. The combined residue clearing and corn kernel loss analysis systems achieved a system accuracy of 0.82 (at 0.90 CI) when known numbers of kernels were hand staged in the row. This system accuracy reflects issues with the residue clearing mower not uncovering kernels or displacing kernels in addition to the accuracy of the image system. Overall accuracy of the system was most affected by the quantity of corn residue left after a residue clearing operation. Tests for assessment of losses using the kernel loss analysis system at different deck plate spacings demonstrated the ability to detect statistically significant ($P < 0.05$) differences in losses between different spacings. The developed systems were able to detect lost corn kernels over a much greater sampling area achieving many more replicate measurements and requiring less labor than previous methods.

CRediT authorship contribution statement

Nolan S. Monhollen: Conceptualization, Methodology, Software, Validation, Formal analysis, Investigation, Writing - original draft. **Kevin J. Shinners:** Conceptualization, Methodology, Formal analysis, Investigation, Writing - review & editing, Resources, Supervision, Project administration, Funding acquisition. **Joshua C. Friede:** Validation, Investigation, Supervision, Resources. **Eduardo M.C. Rocha:** Software, Resources. **Brian L. Luck:** Software, Resources.

Declaration of Competing Interest

The authors declare that they have no known competing financial interests or personal relationships that could have appeared to influence the work reported in this paper.

Acknowledgements

This research was partially sponsored by the University of Wisconsin College of Agriculture and Life Sciences and John Deere Global Crop Harvesting Product Development Center. The authors gratefully acknowledge the cooperation of Gray's Seed Inc., Fairland, IN; University of Wisconsin Arlington Agricultural Research Station and John Deere Horicon Works.

References

Deng, J., Dong, W., Socher, R., Li, L. J., Li, K., & Fei-Fei, L. (2009). Imagenet: A large-scale hierarchical image database. In 2009 IEEE Conference on Computer Vision and Pattern Recognition (pp. 248-255). IEEE.

Escher, M. & T. Krause. (2014). Grain quality camera. In Proceedings of 4th International Conference on Machine Control & Guidance, March 19-20, Braunschweig. https://publikationsserver.tu-braunschweig.de/receive/dbbs_mods_00056119. (Accessed February, 2020).

Hanna, M. (2010) Minimize amount of corn left on the ground behind combine. https://crops.extension.iastate.edu/cropnews/2010/09/minimize-amount-corn-left-ground-behind-combine (Accessed, February, 2020).

Hanna, H.M., Kohl, K.D., Haden, D.A., 2002. Machine losses from conventional versus narrow row corn harvest. Appl. Eng. Agric. 18 (4), 405.

He, K., Zhang, X., Ren, S., & Sun, J. (2016). Deep residual learning for image recognition. In Proceedings of the IEEE Conference on Computer Vision and Pattern Recognition (pp. 770-778). https://arxiv.org/abs/1512.03385 (Accessed, February, 2020).

Li, X., Dai, B., Sun, H., Li, W., 2019. Corn classification system based on computer vision. Symmetry 11 (4), 591.

Monhollen, N.S., 2020. Evaluation of corn header grain loss. Unpublished MS Thesis, Department of Biological Systems Engineering. University of Wisconsin.

Montalvo, M., Guijarro, M., Guerrero, J. M., & Ribeiro, Á. (2016). Identification of plant textures in agricultural images by principal component analysis. In F. Martínez-Álvarez, A. Troncoso, H. Quintián, & E. Corchado (Eds.), Hybrid Artificial Intelligent Systems (pp. 391–401). Springer International Publishing.

Nielsen, R. L. (2018, August). Estimating corn grain yield prior to harvest. https://www.agry.purdue.edu/ext/corn/news/timeless/YldEstMethod.html (Accessed February, 2020).

Orlandi, G., Calvini, R., Foca, G., Ulrici, A., 2018. Automated quantification of defective maize kernels by means of Multivariate Image Analysis. Food Control 85, 259–268.

Paulsen, M.R., Pinto, F.A., de Sena Jr, D.G., Zandonadi, R.S., Ruffato, S., Costa, A.G., Danao, M.G.C., 2014. Measurement of combine losses for corn and soybeans in Brazil. Appl. Eng. Agric. 30 (6), 841–855.

Pearson, T., 2009. Hardware-based image processing for high-speed inspection of grains. Comput. Electron. Agric. 69 (1), 12–18. https://doi.org/10.1016/j.compag.2009.06.007.

Pezzementi, Z., Wellington, C., Tabor, T., Male, C., Herman, H., & Miller, S. (2016). Going against the grain: real-time classification of grain quality. https://research.qut.edu.au/future-farming/wp-content/uploads/sites/3/2018/06/Going-against-the-Grain-Real-Time-Classification-of-Grain-Quality.pdf (Accessed February, 2020).

Pishgar-Komleh, S.H., Keyhani, A., Mostofi-Sarkari, M.R., Jafari, A., 2013. Assessment and determination of seed corn combine harvesting losses and energy consumption. Elixir Agriculture 54 (2013), 12631–12637.

Quick, G. R. (2003). Combine sweet spot: integrating harvested yield, grain damage and losses. In International Conference on Crop Harvesting and Processing (p. 63). American Society of Agricultural and Biological Engineers. ASABE St. Joseph, MI.

Rasmussen, C.B., Moeslund, T.B., 2019. Maize silage kernel fragment estimation using deep learning-based object recognition in non-separated kernel/residue RGB images. Sensors 19 (16).

Ren, S., He, K., Girshick, R., & Sun, J. (2015). Faster R-CNN: Towards Real-Time Object Detection with Region Proposal Networks. In C. Cortes, N. D. Lawrence, D. D. Lee, M. Sugiyama, & R. Garnett (Eds.), Advances in Neural Information Processing Systems 28 (pp. 91–99).

Shauck, T.C., Smeda, R.J., 2011. Factors influencing corn harvest losses in Missouri. Crop Management. https://doi.org/10.1094/CM-2011-0926-01-RS.

Storck, L., Lopes, S.J., Cargnelutti Filho, A., Martini, L.F.D., Carvalho, M.P.D., 2007. Sample size for single, double and thee-way hybrid corn ear traits. Scientia Agricola 64 (1), 30–35.

Valiente-Gonzalez, J.M., Andreu-García, G., Potter, P., Rodas-Jorda, A., 2014. Automatic corn (Zea mays) kernel inspection system using novelty detection based on principal component analysis. Biosyst. Eng. 117, 94–103.